Available online at www.sciencedirect.com
SCIENCE DIRECT®
Engineering Fracture Mechanics 72 (2005) 1830–1840
Engineering Fracture Mechanics
www.elsevier.com/locate/engfracmech

Integral equation approach for 3D multiple-crack problems

S.H. Lo [a,*], C.Y. Dong [b], Y.K. Cheung [a]

[a] Department of Civil Engineering, The University of Hong Kong, Pokfulam Road, Hong Kong, PR China
[b] Department of Applied Mechanics, Beijing Institute of Technology, Beijing 100081, PR China

Received 27 February 2004; received in revised form 30 October 2004; accepted 5 November 2004
Available online 10 March 2005

Abstract

In this paper, a traction integral equation containing no hypersingular integrals is presented to study the interaction of multiple cracks in an infinite elastic medium. 8-node quadratic quadrilateral elements are used to discretize general crack surfaces, and special crack tip elements are employed along surface boundaries to model the $\sqrt{r}$ variation of displacements near the crack fronts. Thus, the method possesses the merits of the traction integral equation without hypersingular integrals and those of the special crack tip elements for modeling $\sqrt{r}$ variation of displacements near the crack tips. The stress intensity factors at the crack front are evaluated using one point formulation and the results are compared with available solutions.

1. Introduction

Cracks present in a structure often cause sudden rapid failure of the structure due to high stresses near the crack tips. In order to understand the failure mechanism due to stress concentration around crack tips, many researches have been carried out. Collins studied two parallel penny-shaped cracks [6] and two coplanar elliptical cracks [5] in an infinite solid using potential theory. Kobayashi et al. [15] used stress functions method to obtain stress intensity factor for an embedded elliptical crack near two parallel free surfaces. Nisitani and Murakami (1974) adopted the body force method to investigate problems of an elliptical crack or a semi-elliptical crack. Isida et al. [14] studied two parallel elliptical cracks located at staggered position in an infinite solid using the body force method. Compared to these methods which are very complicated in their formulations, more well-known numerical methods are the finite element method (FEM) and the boundary element method (BEM). The FEM has been successfully applied to crack problems [12,2].

* Corresponding author. Tel.: +852 28591977; fax: +852 25595337.
E-mail address: hreclsh@hkucc.hku.hk (S.H. Lo).

0013-7944/$ - see front matter © 2005 Elsevier Ltd. All rights reserved.
doi:10.1016/j.engfracmech.2004.11.009

However, its disadvantage is that the problem domain has to be meshed into many finite elements to achieve the required precision. Furthermore, it is not convenient to simulate the crack propagation due to need for remeshing near crack tips. Compared with the FEM, the BEM has some advantages in solving elastic fracture problems. The reason is due to the fact that the BEM only contains the boundary discretization of the problem domain and a more accurate result could be obtained with a lesser effort.

Since Cruse and Vanburen's work [9] about 3D crack problems, the BEM has been widely used to analyze various crack problems. The multidomain BEM [3] involves artificial boundaries along the crack surfaces which are not unique. Thus, it is not convenient to model crack propagation. In addition, it leads to a larger system of equations. The displacement discontinuity method [7] where the unknown functions are the displacement differences between the crack surfaces has been used to solve the crack problems in an infinite domain. However, it is difficult to solve crack problems over a finite domain as higher order kernel functions relative to the conventional BEM are required. The dual boundary element method [13,20,17] is a method in which the displacement integral equation is applied for source points on one of the crack surfaces, whilst the traction integral equation is collocated for source point over the opposite crack surface. As a result, crack problems can be solved with a single domain formulation. However, this method doubles the number of algebraic equations along the cracks. The extended version of the dual boundary element method [19] is a method, in which the displacement integral equation is applied for collocation point outside boundary, while the traction integral equation is applied on one side of the crack surfaces. Thus, doubling of elements and nodes over crack surfaces are avoided as compared with the dual BEM. These dual boundary element methods contain hypersingular integrals which must be carefully evaluated using various regularization techniques, such as Guiggiani et al. [11] and Pan and Amedei [19]. To solve the crack problems more accurately, a direct traction boundary integral equation approach [10] (Dominguez et al., 2000) has been proposed in which the hypersingular and strongly singular integrals are regularized using Taylor's series expansion. All the related hypersingular and strongly singular integrals are transformed into regular or weakly singular integrals by analytical means. These regularization processes are done before boundary discretization. Thus, the corresponding numerical implementation is relatively simple and the accuracy of the results is high due to the avoidance of finite-part integral formulations.

In this paper, the crack-crack interaction in a 3D infinite elastic medium is investigated using a traction integral equation in which the hypersingular integrals are analytically transformed to yield line integrals for planar cracks [10] (Dominguez et al., 2000). In order to accurately simulate the $\sqrt{r}$ variation of the displacement between the upper and the lower crack surfaces, special crack tip elements are employed in the numerical implementation of the traction integral equation. Therefore, the method presented here possesses the merits of both the traction integral equation and those of the special crack tip elements. The proposed method can deal with multiple crack surface of arbitrary geometrical shapes as curved crack surfaces could be meshed into 8-node quadratic quadrilateral elements. Unstaggered equal penny-shaped cracks and coplanar equal penny-shaped cracks are worked out as examples to show the accuracy and effectiveness of the method.

2. Basic formulation

According to Cruse [8], the stress integral equation for a source point P in a 3D infinite medium is given by

$$\sigma_{kl}(P) = \sigma^0_{kl}(P) + \int_S T_{kli}(P;q) D_i(q)\,\mathrm{d}S \tag{1}$$

for k, l, $i = 1, 2, 3$, where S denotes the crack surface, σ^0_{kl} is the stress tensor at the source point P under a remote loading without cracks, $D_i(q) = u_i(q^-) - u_i(q^+)$ in which q^- and q^+ are points of the lower and the upper crack surfaces, T_{kli} is an integral kernel function and can be written as

$$T_{kli} = \frac{E}{8\pi(1-v^2)r^3}\left\{3\frac{\partial r}{\partial n}[(1-2v)\delta_{kl}r_{,i} + v(\delta_{ik}r_{,l} + \delta_{il}r_{,k}) - 5r_{,i}r_{,k}r_{,l}] + 3v(n_k r_{,l}r_{,i} + n_l r_{,k}r_{,i}) + (1-v)(3n_i r_{,k}r_{,l} + n_l\delta_{ki} + n_k\delta_{li}) - (1-4v)n_i\delta_{kl}\right\} \tag{2}$$

where E is the elastic modulus, v is Poisson's ratio, r denotes the distance between the source point P and the field point q, $r_{,i} = \partial r(P;q)/\partial x_i(q)$, n_i is the unit normal vector at the field point q over the crack surfaces, δ_{ij} is the Dirac delta. As $r \to 0$, T_{kli} is hypersingular of order r^{-3}.

When P approaches the crack surface, the corresponding boundary integral equation can be obtained by using the modified geometry at boundary point p taking the appropriate limit (Brebbia and Dominguez, 1992; [10])

$$\sigma_{kl}(p) = \sigma^0_{kl}(p) + \lim_{\varepsilon\to 0}\left\{\int_{S-s_\varepsilon+S_\varepsilon} T_{kli}(p,q)D_i(q)\mathrm{d}\Gamma\right\} \tag{3}$$

where s_ε is a small area near point p. S_ε is a small hemisphere surrounding point p. ε is the radius of the small hemisphere.

From Eq. (3), one can obtain the corresponding traction integral expression

$$t_k(p) = t^0_k(p) + \lim_{\varepsilon\to 0}\left\{\int_{S-s_\varepsilon+S_\varepsilon} T_{kli}(p,q)N_l(p)D_i(q)\mathrm{d}\Gamma\right\} \tag{4}$$

where $t_k(p) = \sigma_{kl}(p)N_l(p)$, $t^0_k(p) = \sigma^0_{kl}(p)N_l(p)$, N_l is the lth component of the unit outward normal at the crack surface.

Considering the property of discontinuity displacement D_i, i.e. $D_i \in C^{1,\alpha}$ (α is a positive constant) at the boundary point p, one has [10]

$$D_i(q) = D_i(p) + D_{i,h}(p)(x_h(q) - x_h(p)) + O(r^{1+\alpha}) \tag{5}$$

Substituting for $D_i(q)$ in Eq. (4) one obtain the following equation

$$t_k(p) = t^0_k(p) + \int_\Gamma T_{kli}N_l[D_i(q) - D_i(p) - D_{i,h}(p)(x_h(q) - x_h(p))]\mathrm{d}\Gamma + \frac{E}{8\pi(1-v^2)}[I_{ki}D_i(p) + J_{khi}D_{i,h}(p)] \tag{6}$$

in which the integral becomes weakly singular of order r^{-1} due to an $O(r^2)$ displacement field. The weakly singular integral of order r^{-1} can be evaluated using Lachat–Watson transformation method [16]. The expressions I_{ki} and J_{khi} can be obtained using the technique presented by Dominguez and Ariza [10]

$$I_{ki} = 3v\oint_\Gamma \frac{\mathbf{r}\times\mathbf{n}}{r^3}r_{,k}r_{,i}\mathrm{d}\boldsymbol{\Gamma} + (1-2v)\delta_{ki}\oint_\Gamma \frac{\mathbf{r}\times\mathbf{n}}{r^3}\mathrm{d}\boldsymbol{\Gamma} + (4v-1)\oint_\Gamma \frac{\mathbf{r}\times\mathbf{e}_i}{r^3}n_k\mathrm{d}\boldsymbol{\Gamma} + (1-2v)\oint_\Gamma \frac{\mathbf{r}\times\mathbf{e}_k}{r^3}n_i\mathrm{d}\boldsymbol{\Gamma} \tag{7}$$

and

$$J_{khi} = v\oint_\Gamma \frac{r_{,k}r_{,h}}{r}(\mathbf{e}_i\times\mathbf{n})\mathrm{d}\boldsymbol{\Gamma} - vn_hn_i\oint_\Gamma \frac{\mathbf{e}_k\times\mathbf{n}}{r}\mathrm{d}\boldsymbol{\Gamma} + vn_kn_i\oint_\Gamma \frac{\mathbf{e}_h\times\mathbf{n}}{r}\mathrm{d}\boldsymbol{\Gamma} + (1-2v)\delta_{ik}\oint_\Gamma \frac{\mathbf{e}_h\times\mathbf{n}}{r}\mathrm{d}\boldsymbol{\Gamma} + v\delta_{ih}\oint_\Gamma \frac{\mathbf{e}_l\times\mathbf{n}}{r}\mathrm{d}\boldsymbol{\Gamma} \tag{8}$$

where Γ is the contour of crack surface S, $\mathbf{e}_k$ is the unit vector along the direction k.

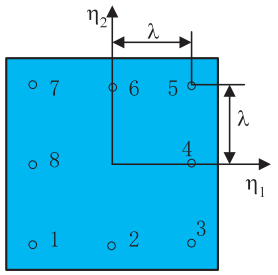

Fig. 1. Eight-node special crack tip element.

Crack surfaces are discretized into 8-node discontinuous elements as shown in Fig. 1. The corresponding shape functions are listed out as follows [1]

$$N_1 = \frac{1}{4\lambda^3}(\lambda - \eta_1)(\lambda - \eta_2)(-\eta_1 - \eta_2 - \lambda) \tag{9a}$$

$$N_2 = \frac{1}{2\lambda^3}(\lambda^2 - \eta_1^2)(\lambda - \eta_2) \tag{9b}$$

$$N_3 = \frac{1}{4\lambda^3}(\lambda + \eta_1)(\lambda - \eta_2)(\eta_1 - \eta_2 - \lambda) \tag{9c}$$

$$N_4 = \frac{1}{2\lambda^3}(\lambda + \eta_1)(\lambda^2 - \eta_2^2) \tag{9d}$$

$$N_5 = \frac{1}{4\lambda^3}(\lambda + \eta_1)(\lambda + \eta_2)(\eta_1 + \eta_2 - \lambda) \tag{9e}$$

$$N_6 = \frac{1}{2\lambda^3}(\lambda^2 - \eta_1^2)(\lambda + \eta_2) \tag{9f}$$

$$N_7 = \frac{1}{4\lambda^3}(\lambda - \eta_1)(\lambda + \eta_2)(-\eta_1 + \eta_2 - \lambda) \tag{9g}$$

$$N_8 = \frac{1}{2\lambda^3}(\lambda - \eta_1)(\lambda^2 - \eta_2^2) \tag{9h}$$

In order to model the $\sqrt{r}$ variation of the discontinuous displacements near the crack front, special 8-node crack tip elements are used [18], and their shape functions are given by

$$N^b = a_1^b + a_2^b\xi + a_3^b\sqrt{1+\eta} + a_4^b\xi\sqrt{1+\eta} + a_5^b\xi^2 + a_6^b(1+\eta) + a_7^b\xi^2\sqrt{1+\eta} + a_8^b\xi(1+\eta) \tag{10}$$

for $b = 1,2,\ldots,8$ (see Fig. 1), the eight coefficients $a_j^b (j = 1,2,\ldots,8)$ can be obtained by solving a system of eight linear equations which has the following properties: $N^b = 1$ for the collocation point b; $N^b = 0$ for the seven remaining collocation points. For ease of reference, these shape functions are listed below [1]

$$\begin{aligned} N_1 = \{&(-\lambda + \eta_1)[-\lambda p + \lambda^2(1-q) - (1-q)(1+q+2\lambda q) + (-3p + (1+\lambda)(2-q) + 2pq)\eta_1 \\ &+ (\lambda^2 + \lambda(1-p)(3-q))s + (3-2p-2q+pq)\eta_1 s + (\lambda(2-p) + (1-p)(1+q))s^2]\}/(-2\lambda D) \end{aligned} \tag{11a}$$

$$N_2 = \{(\lambda-\eta_1)(\lambda+\eta_1)[-2\lambda-2\lambda^2+3\lambda p+\lambda q+\lambda^2 q-2\lambda pq+(-3\lambda+2\lambda p+2\lambda q-\lambda pq)s]\}/(\lambda^2 D) \tag{11b}$$

$$N_3 = \{(-\lambda-\eta_1)[-\lambda p+\lambda^2(1-q)-(1-p)(1+q+2\lambda q)+(3p-(1+\lambda)(2-q)-2pq)\eta_1 + (\lambda^2+\lambda(1-p)(3-q))s+(-3+2p+2q-pq)\eta_1 s+(\lambda(2-p)+(1-p)(1+q))s^2]\}/(-2\lambda D) \tag{11c}$$

$$N_4 = \{(\lambda+\eta_1)[4\lambda+2\lambda p(-\lambda+\lambda^2-2q)+2\lambda^2(-2\lambda+q+\lambda q)+4\lambda^2(-\lambda+p-q)s + (2\lambda^2(p-q)+4\lambda(pq-1))s^2]\}/(4\lambda^2 D) \tag{11d}$$

$$N_5 = \{-(\lambda+\eta_1)[2\lambda(1-\lambda^2+p-2\lambda p+\lambda^2 p-q-\lambda q-pq+2\lambda pq)-2\lambda(2-2\lambda-p+\lambda p-3q+2pq)\eta_1 - 2\lambda^2(-3+\lambda+p+3q-pq)s-2\lambda(3-2p-2q+pq)\eta_1 s - 2\lambda(1-2\lambda+p-q+\lambda q-pq)s^2]\}/(4\lambda^2 D) \tag{11e}$$

$$N_6 = \{(-\lambda-\eta_1)(\lambda-\eta_1)[-2\lambda+2\lambda^2+\lambda p-\lambda^2 p+3\lambda p-2\lambda pq+(-3\lambda+2\lambda p+2\lambda q-\lambda pq)s]\}/(\lambda^2 D) \tag{11f}$$

$$N_7 = \{-(\lambda-\eta_1)[2\lambda(1-\lambda^2+p-2\lambda p+\lambda^2 p-q-\lambda q-pq+2\lambda pq) + 2\lambda(2-2\lambda-p+\lambda p-3q+2pq)\eta_1-2\lambda^2(-3+\lambda+p+3q-pq)s-2\lambda(3-2p-2q+pq)\eta_1 s - 2\lambda(1-2\lambda+p-q+\lambda q-pq)s^2]\}/(4\lambda^2 D) \tag{11g}$$

$$N_8 = \{(\lambda-\eta_1)[4\lambda+2\lambda p(-\lambda+\lambda^2-2q)+2\lambda^2(-2\lambda+q+\lambda q)+4\lambda^2(-\lambda+p-q)s+(2\lambda^2(p-q) + 4\lambda(pq-1))s^2]\}/(4\lambda^2 D) \tag{11h}$$

From the above discretization process, one can obtain a system of equations as follows

$$\mathbf{AD} = \mathbf{F} \tag{12}$$

where **A** is a coefficient matrix, **F** is a column vector containing known values, and **D** is a column vector containing the discontinuous displacement components over the cracks.

Once the discontinuous displacements are available, the stress intensity factors along the crack front can be calculated by [1]

$$\begin{cases} K_{\mathrm{I}} = \dfrac{E}{4(1-\nu^2)}\sqrt{\dfrac{\pi}{2r}}D_n \\ K_{\mathrm{II}} = \dfrac{E}{4(1-\nu^2)}\sqrt{\dfrac{\pi}{2r}}D_{t_1} \\ K_{\mathrm{III}} = \dfrac{E}{4(1-\nu^2)}\sqrt{\dfrac{\pi}{2r}}D_{t_2} \end{cases} \tag{13}$$

where r is the shortest distance from the calculation point p to the nearest crack front, the corresponding point of which is taken as q. D_n, D_{t_1} and D_{t_2} are respectively discontinuous displacement components along the local coordinate system at point q as shown in Fig. 2.

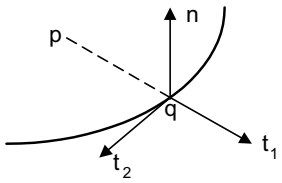

Fig. 2. Local coordinate system at point q.

3. Numerical examples

3.1. Example 1: Equal penny-shaped cracks

Fig. 3(a) shows an infinite elastic medium containing two unstaggered equal penny-shaped cracks under a remote loading ($\sigma^0 = 1$) along the z-direction. The material parameters are as follows: $E = 1000$, $v = 0.3$. Each crack surface of radius $a = 1$ is meshed into 64 eight-node quadratic quadrilateral elements in which 16 eight-node special quadratic quadrilateral elements (elements shaded) are distributed along the crack front as shown in Fig. 3(b).

The stress intensity factors are listed in Table 1, together with the results from Isida et al. [14]. From Table 1, we found that the results from the present method are in good agreement with those obtained by Isida et al. [14] using the body force method.

3.2. Example 2: Two coplanar equal cracks

Two coplanar equal penny-shaped cracks in an infinite elastic medium under a remote loading ($\sigma^0 = 1$) along the z-direction is shown in Fig. 4. The material data are: the elastic modulus $E = 1000$, Poisson's ratio

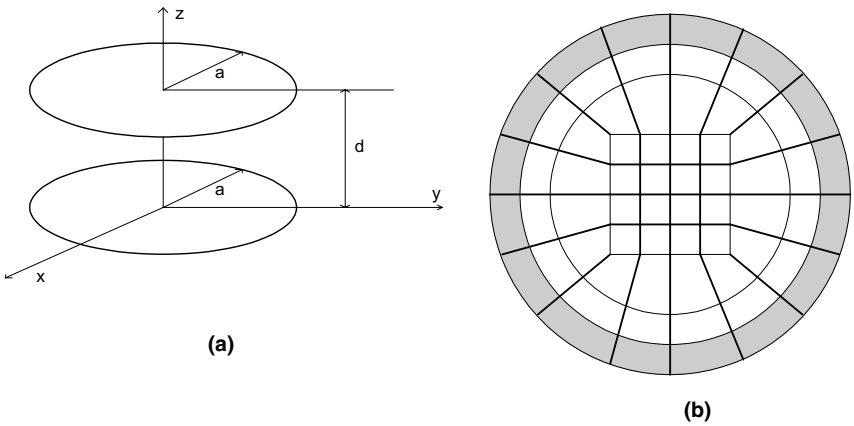

Fig. 3. (a) Two parallel penny-shaped cracks; (b) mesh division of crack surfaces.

Table 1
Stress intensity factor at crack front $\left(\frac{K_I}{\sigma\sqrt{\pi a}}\right)$

$d/(2a)$	0.5	0.75	1.0	1.5	2.0	5.0
Isida et al. [14]	0.532	0.562	0.585	0.612	0.624	0.636
Present	0.524	0.558	0.583	0.610	0.622	0.633

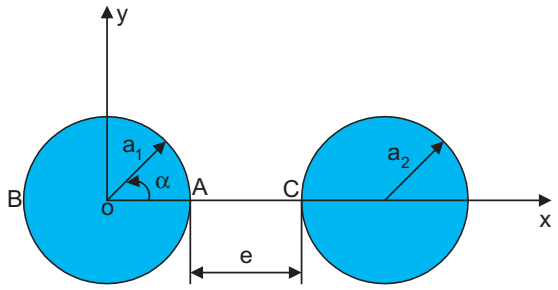

Fig. 4. Two coplanar penny-shaped cracks.

$v = 0.3$. The distance e between A and C can be varied. Each crack surface is meshed in exactly the same way as the previous example as shown in Fig. 3(b). The radius of each crack surface is $a_1 = a_2 = 1$. For different values of e, the stress intensity factors along the arc AB are shown in Fig. 5. It can be found that the smaller the distance e between A and C, the greater the change of stress intensity factor along arc AB. Near point B, the influence of the distance e between A and C on the stress intensity factor is smaller. Chen, Hasebe and Lee [4] used hypersingular integral equation approach to study the same problem, the results of which are also plotted out in Fig. 5. One can observe that their results are in good agreement with our results. Note here that the results presented by Chen, Hasebe and Lee [4] have been normalized by the factor $\frac{K_I}{\sigma\sqrt{\pi a}}$ for comparison. For $e = 0.5$ and different radii of the second penny-shaped crack, the stress intensity factors along arc AB are shown in Fig. 6. As expected, one can find that the stress intensity factor becomes larger as radius *a2* increases.

3.3. Example 3: Three coplanar cracks

Fig. 7 shows three coplanar penny-shaped cracks in an infinite elastic medium under a remote loading ($\sigma^0 = 1$) along the z-direction. The material data are: the elastic modulus $E = 1000$, Poisson's ratio $v = 0.3$. The distance e between A and C is set equal to 2. The division of crack surface is the same as the above two examples as shown in Fig. 3(b). Three radii of the crack surfaces are respectively $a_1 = a_2 = 1$ and $a_3 = 0.5$. The distances of the crack center o_3 to x-axis and y-axis are h and b respectively, while b is kept constant

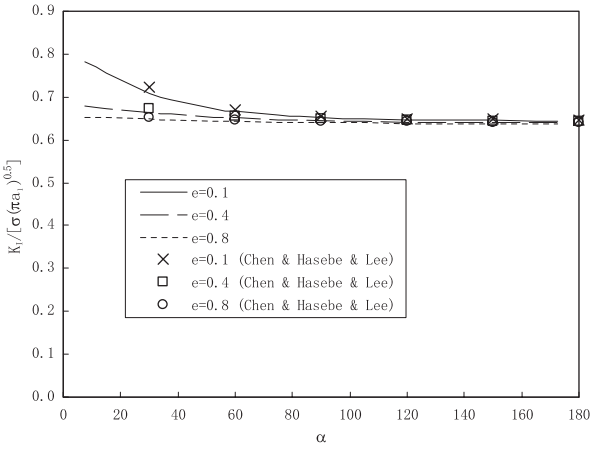

Fig. 5. Normalized stress intensity factor along arc AB at crack front for different angle α and e.

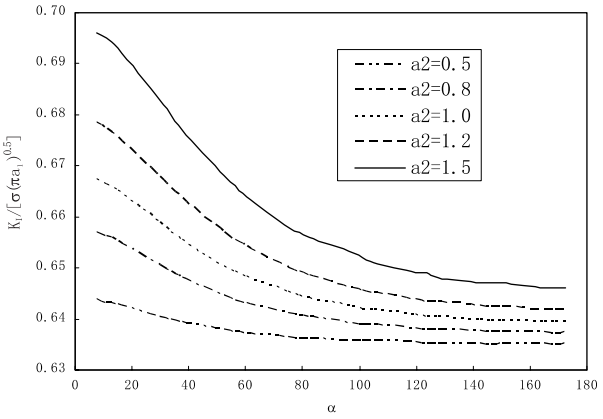

Fig. 6. Normalized stress intensity factor along arc AB at crack front for different angle α and *a*2.

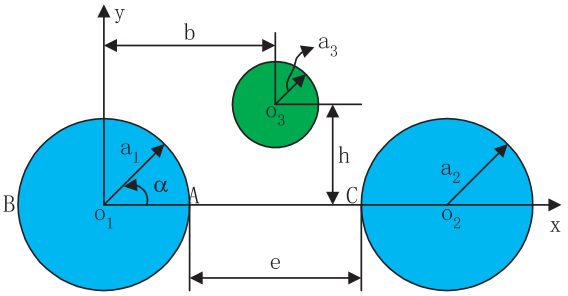

Fig. 7. Three coplanar penny-shapes cracks.

($b = 2$), the value of h could be varied. For different values of h, the stress intensity factor along arc AB is shown in Fig. 8. One can find that the strong change of the stress intensity factor along arc AB happens near point A as expected. As h is increased, the effect of the third crack on the other two cracks gradually

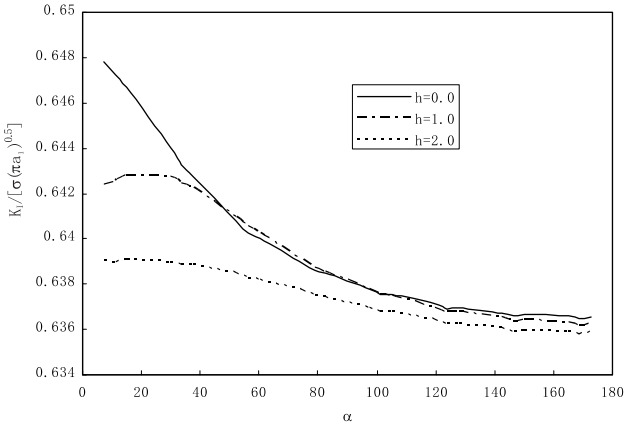

Fig. 8. Normalized stress intensity factor at crack front against angle α.

diminished. Since the solution of the same problem cannot be found in the available references, our results can be taken as a reference solution for other investigators.

3.4. Example 4: Three staggered equal penny-shaped cracks

Three staggered equal penny-shaped cracks in an infinite elastic medium under a remote loading ($\sigma^0 = 1$) along the z-direction is shown in Fig. 9. The material data are: the elastic modulus $E = 1000$, Poisson's ratio $v = 0.3$. The distance d between cracks 1 and 2 is taken to be 1. The discretization of crack surfaces is the same as the previous examples as shown in Fig. 3(b). The radius of each crack surface is set equal to 1, i.e. $a_1 = a_2 = a_3 = 1$. The center coordinates of the third crack surface is taken as (0.0, e, 0.5), in which e varies. For different values of e, the stress intensity factor along arc AB is shown in Fig. 10. As expected, it can be

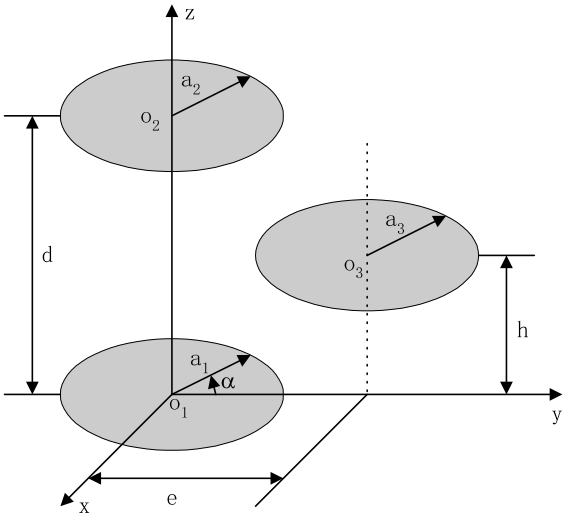

Fig. 9. Three unstaggered equal penny-shapes cracks.

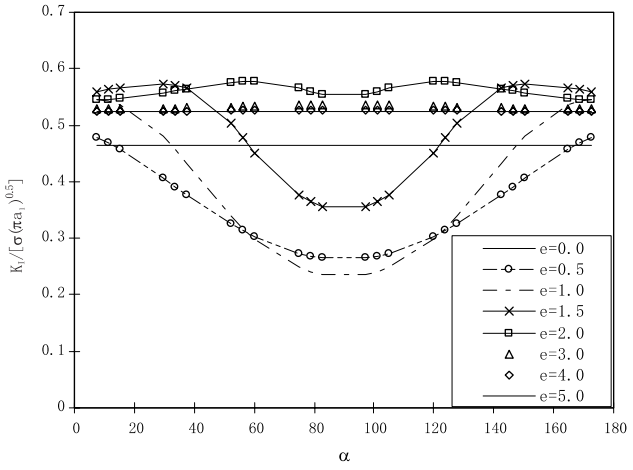

Fig. 10. Normalized stress intensity factor at crack front against angle α.

found that the stress intensity factor almost remains the same for $e = 0.0$. As e is increased, the stress intensity factor along arc AB shows a parabolic variation. Especially, when $e \geqslant 4.0$, the stress intensity factor along arc AB remains almost constant at a value of 0.524 which is the same as the first example. This shows that the effect of the third crack on cracks 1 and 2 disappears when $e \geqslant 4.0$. To the best knowledge of the authors, this result has not been published in the literature.

4. Conclusion

Based on a regularized traction integral equation containing no hypersingular integrals, the problems of unstaggered cracks and coplanar penny-shaped cracks within a 3D elastic medium have been investigated. The stress intensity factors along the tip of the crack surfaces have been evaluated. The present results are in good agreement with those from other methods. Problems involving three crack surfaces lying on a plane or in a staggered arrangement have also been worked out as reference solutions.

Acknowledgement

The work described in this paper was partially supported by a grant from the Research Grant Council of the Hong Kong Special Administration Region, China (Project No.: HKU 7011/01E).

References

[1] Aliabadi MH. The boundary element method. John Wiley & Sons, Ltd; 2002.
[2] Barsoum RS. On the use of isoparametric finite elements in linear fracture mechanics. Int J Numer Meth Engng 1976;10:25–37.
[3] Blandford GE, Ingraffea AR, Liggett JA. Two-dimensional stress intensity factor computations using the boundary element method. Int J Numer Meth Engng 1981;17:387–404.
[4] Chen YZ, Hasebe N, Lee KY. Multiple crack problems in elasticity. Southampton: WIT Press; 2003.
[5] Collins WD. Some coplanar punch and crack problems in three-dimensional elastics. Proc Royal Soc London A 1963;274:507–28.
[6] Collins WD. Some axially symmetric stress distributions in elastic solids containing penny-shaped cracks. I. Cracks in an infinite solid and a thick plate. Proc Royal Soc London A 1962;266:359–86.
[7] Crouch SL. Solution of plane elasticity problems by the displacement discontinuity method. Int J Numer Meth Engng 1976;10:301–42.
[8] Cruse TA. Boundary element analysis in computational fracture mechanics. Dordrecht: Kluwer Academic; 1988.
[9] Cruse TA, Vanburen W. Three dimensional elastic stress analysis of a fracture specimen with an edge crack. Int J Fract 1971;17:1–15.
[10] Dominguez J, Ariza MP. A direct traction BIE approach for three-dimensional crack problems. Engng Anal Boundary Elements 2000;24:727–38.
[11] Guiggiani M, Krishnasamy G, Rudolphi TJ, Rizzo FJ. General algorithm for the numerical solution of hypersingular boundary integral equations. J Appl Mech ASME 1992;59:604–14.
[12] Henshell RD, Shaw KG. Crack tip finite elements are unnecessary. Int J Numer Meth Engng 1975;9:495–507.
[13] Hong H, Chen J. Derivation of integral equations of elasticity. J Engng Mech ASCE 1988;114:1028–44.
[14] Isida M, Hirota K, Noguchi H, Yoshida T. Two parallel elliptical cracks in an infinite solid subjected to tension. Int J Fract 1985;27:31–48.
[15] Kobayashi AS, Ziv M, Hall LR. Approximate stress intensity factor for an embedded elliptical crack near two parallel free surfaces. Int J Fract Mech 1965;1:81–95.
[16] Lachat JC, Watson JO. Effective numerical treatment of boundary integral equations: a formulation for three-dimensional elastostatics. Int J Numer Meth Engng 1976;10:991–1005.
[17] Mi Y, Aliabadi MH. Dual boundary element method for three-dimensional fracture mechanics analysis. Engng Anal Boundary Elem 1992;10:161–71.
[18] Mi Y. Three-dimensional analysis of crack growth. Southampton: Computational Mechanics Publications; 1996.

[19] Pan E, Amadei B. Fracture mechanics analysis of 2-D cracked anisotropic media with a new formulation of the boundary element method. Int J Fract 1996;77:161–74.

[20] Portela A, Aliabadi MH, Rooke DP. The dual boundary element method: effective implementation for crack problems. Int J Numer Meth Engng 1992;33:1269–87;
Nisitani H, Murakami Y. Strees intensity factors of an elliptical crack or semielliptical crack subject to tension. Int J Fract 1974;10(3):353–68.